

# REPORT DOCUMENTATION PAGE

*Form Approved*  
**OMB No. 0704-0188**

Public reporting burden for this collection of information is estimated to average 1 hour per response, including the time for reviewing instructions, searching existing data sources, gathering and maintaining the data needed, and completing and reviewing this collection of information. Send comments regarding this burden estimate or any other aspect of this collection of information, including suggestions for reducing this burden to Department of Defense, Washington Headquarters Services, Directorate for Information Operations and Reports (0704-0188), 1215 Jefferson Davis Highway, Suite 1204, Arlington, VA 22202-4302. Respondents should be aware that notwithstanding any other provision of law, no person shall be subject to any penalty for failing to comply with a collection of information if it does not display a currently valid OMB control number. **PLEASE DO NOT RETURN YOUR FORM TO THE ABOVE ADDRESS.**

<b>1. REPORT DATE (DD-MM-YYYY)</b> 18-01-2005		<b>2. REPORT TYPE</b> Final Technical		<b>3. DATES COVERED (From - To)</b> 01-03-2001 - 30-09-2004	
<b>4. TITLE AND SUBTITLE</b> Breakdown behavior of fuels for pulsed detonation engines				<b>5a. CONTRACT NUMBER</b>	
				<b>5b. GRANT NUMBER</b> N00014-01-1-0541	
				<b>5c. PROGRAM ELEMENT NUMBER</b>	
<b>6. AUTHOR(S)</b> Scott L. Anderson				<b>5d. PROJECT NUMBER</b>	
				<b>5e. TASK NUMBER</b>	
				<b>5f. WORK UNIT NUMBER</b>	
<b>7. PERFORMING ORGANIZATION NAME(S) AND ADDRESS(ES)</b>  University of Utah 1471 Federal Way Salt Lake City UT 84112				<b>8. PERFORMING ORGANIZATION REPORT NUMBER</b>  None	
<b>9. SPONSORING / MONITORING AGENCY NAME(S) AND ADDRESS(ES)</b> Dr. Gabriel Roy ONR Mechanics Division 800 N. Quincy St. Arlington, VA 22217				<b>10. SPONSOR/MONITOR'S ACRONYM(S)</b> ONR	
				<b>11. SPONSOR/MONITOR'S REPORT NUMBER(S)</b>	
<b>12. DISTRIBUTION / AVAILABILITY STATEMENT</b>  unlimited					
<b>13. SUPPLEMENTARY NOTES</b>  Micro flow tube mass spectrometry has been used to analyze the thermal breakdown behavior of JP-10, with and without oxygen present. In the final project period, catalytic enhancement of JP-10 pyrolysis by nano-powdered catalysts was studied					
<b>15. SUBJECT TERMS</b> Fuels, JP-10, catalysis, combustion					
<b>16. SECURITY CLASSIFICATION OF:</b>			<b>17. LIMITATION OF ABSTRACT</b>  Unlimited	<b>18. NUMBER OF PAGES</b>  21	<b>19a. NAME OF RESPONSIBLE PERSON</b> Scott L. Anderson
<b>a. REPORT</b> None	<b>b. ABSTRACT</b> None	<b>c. THIS PAGE</b> None			<b>19b. TELEPHONE NUMBER (include area code)</b> (801) 585-7289

**Institution:** Department of Chemistry  
University of Utah  
315 S. 1400 E. Rm 2020  
Salt Lake City, UT 84112

**Title:** Breakdown behavior of fuels for pulsed detonation engines

**Technical Contact/PI:** Scott L. Anderson  
Department of Chemistry  
University of Utah  
315 S. 1400 E. Rm 2020  
Salt Lake City, UT 84112  
(801) 585-7289  
(801) 581-8433 (FAX)  
anderson@chem.utah.edu

**Administrative Contact:** Vincent Bogdanski  
1471 Federal Way  
Salt Lake City, UT 84102  
(801) 581-6903  
(801) 581-3007 (fax)  
ospawards@osp.utah.edu

#### ABSTRACT

Decomposition of JP-10 (exo-tetrahydodicyclopentadiene) was studied in a small flow tube reactor over the temperature range up to  $\sim 1700$  K on the millisecond time scale. For comparison, the decomposition behavior of adamantane, cyclopentadiene, dicyclopentadiene, and benzene were studied under identical conditions. Products of pyrolysis were identified by chemical ionization (CI) and electron ionization (EI) mass spectrometry. On the experimental time scale, JP-10 begins to decompose above 900K, and is completely decomposed by 1300K. In the initial decomposition, the principal products are cyclopentadiene, benzene, propyne, and  $C_4H_x$ . At high temperatures, the cyclopentadiene decomposes, and the principal species observed are benzene, acetylene, and ethylene. From the combination of EI and CI spectra, we can confirm that the  $C_6$  product observed is benzene, with little if any other  $C_6H_x$  products. Similarly, the  $C_5$  product is cyclopentadiene, with no cyclopentene or other  $C_5H_x$  products. The observed product distribution is inconsistent with both equilibrium speciation and predictions of existing JP-10 kinetic models.

In the final project period, a study of catalytic effects of nanoparticle additives on JP-10 breakdown and oxidation was initiated. Substantial acceleration of JP-10 breakdown rates are observed for  $CeO_2$  loadings consistent with average JP-10 - particle collision numbers around 10. In addition, the product distribution is dramatically altered, compared to the uncatalyzed case, where hydrocarbon fragments predominate in the initial breakdown. Instead, the catalyzed reaction yield oxidation products such as water, CO,  $CO_2$ , and  $H_2CO$ .

20050125 155

In the following, separate sections report the results on JP-10 pyrolysis, and on nanocatalysis effects.

### JP-10 Pyrolysis Section (uncatalyzed):

JP-10 is a synthetic high energy density fuel used in missile applications and in many combustion research studies.<sup>1-15</sup> It is chiefly composed of a single compound, exo-tetrahydrodicyclopentadiene (exo-THDCP, IUPAC name: tricyclo[5.2.1.0<sup>2,6</sup>]decane), and therefore is simpler to study than typical refined hydrocarbon fuels, which are complex mixtures that may vary from source-to-source. Good data are available on thermochemical, rheological, and other physical properties.<sup>2,4,16-23</sup> On the other hand, there is relatively little known regarding the detailed combustion mechanism. Rate constants have been reported for reaction of JP-10 with OH, O<sub>2</sub>, and O<sub>3</sub>,<sup>4,17,20</sup> but only at room temperature. Shock tube measurements have been performed on JP-10 ignition, which provide information on the kinetics of the combustion but not detailed information about the chemical species involved.<sup>24,25</sup> Williams and co-workers<sup>1</sup> have suggested a mechanism, in which the first step of THDCP breakdown proceeds by breaking a C-C bond common to two five-membered rings, and eventual breakdown to acetylene and ethylene. Davidson et al.<sup>25</sup> conclude from shock-tube measurements and kinetic modeling that C<sub>2</sub> species probably play an important role in the decomposition of JP-10. Information regarding product speciation as a function of temperature is important, both in guiding development of combustion models, and in development and interpretation of optical diagnostics for JP-10 ignition/combustion. Our experiments are aimed at providing this information.

### EXPERIMENTAL APPROACH

The micro-Flow Tube Reactor/Mass Spectrometer instrument (micro-FTRMS) has been described in detail in previous publications on pyrolysis of quadricyclane and cubanes.<sup>26,27</sup> To work at the higher temperatures needed to decompose JP-10, the quartz flow tube was replaced with an alumina tube (2.39 mm ID) heated by external tantalum windings, capable of prolonged operation at 1800K. The alumina tube is ~30 cm long, but only the final ~10 cm is heated, allowing transition to laminar flow prior to entering the hot zone. During reaction runs, the temperature is measured continuously by a thermocouple embedded against the outside wall of the alumina tube. To calibrate this external thermocouple, separate calibration runs were carried out periodically, in which a second thermocouple was inserted inside the flow tube bore. Both temperatures were measured simultaneously and a calibration curve was constructed, accurate to ±2K. The inside thermocouple was removed during reaction runs to avoid reactions on the metal thermocouple surfaces. By building a flow tube with several external thermocouples, and periodically checking the external measurements against a thermocouple that can be inserted into the flow tube bore, we conclude that the temperature is constant over 90% of the hot zone length.

The flow-tube exhaust is dumped into a sealed, temperature stabilized (~200°C) ionization source where analyte molecules can be ionized either by electron impact ionization (EI), or by methane chemical ionization (CI). The total source pressure is either 0.35 or 1.5 Torr, for EI and CI, respectively. The flow tube is inserted into a 3 mm deep counterbore in the ion source, such that it does not make direct contact. There is a 0.05 mm annular gap between the flow tube and counterbore, creating a connection with low thermal conductivity but also with low conductance for gas loss. The main points whereby gas can exit the source are a via the 0.99 mm orifice where ions exit the source, and a 0.55 mm orifice where a magnetically collimated electron beam is injected into the source to cause ionization. For EI, the electron beam ionizes the analyte molecules directly. For CI, methane is injected into the source through a separate inlet, avoiding the possibility of reactions between methane and the gas flow in the hot zone of the flow tube. Electrons are injected into the source, where they predominantly ionize the methane, although there is undoubtedly also some EI of analyte molecules. Ion-molecule reactions in the methane generate a series of low mass hydrocarbon reagent ions, the most abundant being CH<sub>5</sub><sup>+</sup>. In collisions with most molecules (M), the proton transfer reaction:  $M + CH_5^+ \rightarrow (M+H)^+ + CH_4$  is exoergic, and proceeds on every collision (see below). The advantage of CI is that it is a relatively gentle ionization method. For

many molecules, CI results in a spectrum consisting primarily of the  $(M+H)^+$  ion, making identification of the parent mass (M) trivial. A major disadvantage of CI is that the low mass region of the CI spectrum is dominated by the hydrocarbon reagent ions, interfering with detection of low mass species. In addition, CI spectra, while quite reproducible in any given instrument, vary significantly with ion source design and operating conditions. For this reason no database of "standard" CI spectra is available to aid spectral assignments. Analysis of EI spectra is complicated by extensive fragmentation, however, standard spectral libraries are available to guide identification.<sup>28</sup> After exiting the ion source, the ions are analyzed by a tandem mass spectrometer, operated for these experiments as a single stage mass spectrometer.

Argon or helium is bubbled through JP-10 at room temperature, generating a reactant flow that is ~7 % JP-10. The reactant mix is metered through a glass/teflon leak valve into the flow tube, where the pressure drops into the Torr range. Because this valve is not adjusted during a set of experiments, the total mass flow rate through the reactor is independent of temperature, as verified by constant vacuum system gas load. On the other hand, the hot zone gas density and flow velocity do change with flow tube temperature. The density, pressure, and flow velocity at the flow tube mid point, together with the calculated hot zone residence time, are shown in Table I. Flow properties were calculated assuming incompressible flow, which is reasonable in light of the low flow velocities. Flow properties differ by ~50% under CI and EI analysis conditions, because of the methane injected into the ion source during CI.

From the density and gas (mostly Ar or He) viscosity, the diffusion constant can be calculated, and used to estimate the average distance the JP-10 molecules will diffuse during the residence time in the hot zone. This turns out to be 50 to 70 mm for EI conditions, and 20 to 30 mm for CI conditions. This diffusion length is substantially larger than the flow tube diameter, thus the JP-10 molecules clearly diffuse across the tube bore many times during passage through the hot zone. There are several consequences. The flow can be treated as pseudo-plug flow, i.e., all sample molecules have equal residence times in the hot zones. In addition, collisions with the flow tube wall mean that the JP-10 molecular temperature should track the wall temperature quite closely.

Wall collisions also lead to the possibility of wall-catalyzed reactions. We have examined chemistry in both alumina and silica tubes, and also in a tube with larger diameter and faster flow velocities, where the number of wall collisions is smaller. The product distributions are essentially identical in all cases, at least up to the maximum working temperature of the silica tube (~1300 K). The tube walls are observed to develop a light grey color during the initial pyrolysis run, presumably because of carbon deposition on the walls. Once this carbon layer forms, it does not thicken noticeably in months of operation. The only suggestion of unique wall chemistry in the JP-10 system is that various primary products are observed to undergo dehydrogenation at temperatures above 1500K, and this chemistry probably is wall catalyzed. We conclude that there is substantial wall chemistry for clean silica or alumina surfaces, but that carbon deposition rapidly passivates the surface, and wall chemistry thereafter is important only at temperatures well above the breakdown temperature of JP-10.

Two samples of JP-10, both obtained from Koch petroleum, were examined. Prior to analysis in the flow tube reactor, both samples were analyzed for purity via a gas chromatography-mass spectrometry (GC-MS). One sample was commercial, mil-spec JP-10, which includes stabilizers. This sample elutes from the GC in four major components with elution times from 4.5 to 5 minutes. The main peak at 4.72 minutes is identified as the exo-THDCP isomer, and gives a mass spectrum similar to those shown below. Another peak, eluting at just over 5 minutes, has a nearly identical mass spectrum, and is therefore identified as the endo-THDCP isomer. The other two GC peaks give mass spectra with major peaks near the molecular weight of exo-THDCP (136 amu), however there is considerably less fragmentation, suggesting that these contaminants are less strained isomers. This commercial sample was estimated to be ~75 % exo-THDCP. To avoid complications from the endo isomer and other contaminants, all the flow tube reaction data below was taken using a sample of freshly-synthesized, unstabilized JP-10 that was distilled by Koch Petroleum to higher purity than the commercial-grade product. GC-MS analysis shows this sample to be about 96% pure exo-THDCP.

A few authors have studied the mass spectra of exo-THDCP.<sup>18,19</sup> Inman et al.<sup>18</sup> studied the fragmentation of exo-THDCP with electron impact ionization (EI) at 70 eV after gas chromatographic

separation. They found large fragment peaks at masses 121, 95, 94, 79 and 67. Herzshuh et. al.<sup>19</sup> also studied the EI fragmentation pattern at electron energies of both 70 and 14 eV. At 70 eV, the parent peak is only at 8.4%, but grows to 36.9% at 14 eV. At 14 eV, they find large fragment peaks at 121, 108, 95, 94, and 66 amu. Our EI mass spectrometry results below are generally consistent with the previous data. The small differences probably reflect differences in EI conditions, such as source pressure and temperature, and presence of He buffer gas in our EI experiments.

## RESULTS AND DISCUSSION

### The CI fingerprint of JP-10

Pyrolysis studies were conducted on the high purity JP-10 sample, and also on related compounds considered to be possible products of JP-10 pyrolysis. Comparison of the temperature-dependent mass spectra of these compounds with the JP-10 pyrolysis mass spectra, allows us to assign the identity of the products with reasonable confidence. The EI data discussed in the next section provide corroborating evidence, and allow examination of the low mass reaction of the product distribution. Fig. 1 shows a series of methane chemical ionization (CI) mass spectra after passing JP-10 in argon through the flow tube at different temperatures (Right hand scale). To improve visibility of the weak peaks present at masses above 100 amu, this region of the mass spectra has been scaled up by a factor of 15. The spectra were actually scanned over the mass range up to 300 amu, to check for adducts or species that might result from polymerization on the flow tube walls. No significant peaks are observed above 140 amu.

The bottom spectrum is for the flow tube at room temperature (right hand scale), where no decomposition occurs. This spectrum shows the CI fingerprint of JP-10, itself, i.e., all the mass peaks observed result from CI of intact JP-10 entering the ion source. In addition to a weak molecular mass peak (136 amu), the CI mass spectrum is dominated by a characteristic set of fragment ion peaks. The important CI fragment masses, and the corresponding net atom losses from  $(M+H)^+$ , are 135 ( $-H_2$ ), 95 ( $-C_3H_6$ ), 81 ( $-C_4H_8$ ) and 67 ( $-C_5H_{10}$ ). There is also a prominent peak at 41 ( $C_3H_5^+$ ), corresponding to loss of  $C_7H_{12}$  from  $(M+H)^+$ . Mass 41 is also prominent in the background spectrum of hydrocarbon CI reagent ions, however, the changes in mass 41 intensity with temperature indicate real signal at this mass. This conclusion is verified by the EI spectra (below).

It is somewhat unusual for a molecule to fragment so extensively in CI. Mass spectral data provide no information on fragmentation pathways, e.g., loss of  $C_5H_{10}$  could come from any combination of neutral species adding up to the correct mass. Nonetheless, it is possible to rationalize the observed pattern theoretically. To help understand the JP-10 fragmentation, we carried out the following *ab initio* calculations, using GAUSSIAN 98.<sup>29</sup> The JP-10 (i.e., exo-THDCP) structure was first optimized at the B3LYP/6-31G\* level of theory, then the effect of protonation (the dominant ionization pathway in methane CI) was examined in two steps. In the first step, a proton was added to one of the six distinguishable carbon atom sites in JP-10 then the geometry was reoptimized with the carbon skeleton frozen. The energy difference between the resulting structures and the JP-10 structure gives a rough estimate of the vertical proton affinity (i.e., the proton affinity in absence of isomerization/skeletal relaxation). The values are quite similar for all carbon sites, ranging from 6.87 eV to 6.54 eV. From the point of view of detection efficiency, the important point is that the adiabatic proton affinities at all carbon sites are significantly larger than that of  $CH_4$  (5.49 eV<sup>30</sup>) so that the proton transfer ionization process should be efficient. Because the energies are so similar, it is not unreasonable to assume that protonation occurs at every site, depending mainly on collision orientation.

Each geometry was then reoptimized with all atoms free to move. The resulting structures provide insight into the protonation-induced fragmentation processes, and provide adiabatic proton affinities, which range from 6.6 eV to 8.7 eV. Protonation is calculated to result in dramatic site-dependent changes in JP-10 structure, and the resulting structures allow us to rationalize the main features of the observed fragmentation pattern.

### Variable temperature CI - JP-10 Pyrolysis

In Fig. 1, the mass spectra are temperature independent for  $T < 1000\text{K}$ , but at higher temperatures changes in the mass spectra indicate that JP-10 is breaking down. In particular, certain peaks characteristic of JP-10 (e.g. mass 81, the group of peaks at 135 - 137) decrease in intensity, disappearing completely above  $\sim 1300\text{K}$ . The disappearance of these peaks indicates that JP-10 decomposes on the millisecond time scale in this temperature range. At the same time, new peaks grow in, indicating the presence of pyrolysis products. There is a group around mass 55, corresponding to  $\text{C}_4$  species, a large peak at mass 79, corresponding to  $\text{C}_6\text{H}_7^+$ , and peaks at 91 and 93 corresponding to  $\text{C}_7$  products. There are also groups of peaks corresponding to  $\text{C}_8$ ,  $\text{C}_9$ , and  $\text{C}_{10}$  products, however, these contribute a negligible fraction of the total product signal (note 15x scale change at mass 100). Some mass peaks clearly appear in the spectra of both JP-10 and its pyrolysis products. For example, mass 67, corresponding to  $\text{C}_5\text{H}_7^+$ , is a major peak in the JP-10 spectra at low temperatures, but also appears (with increased intensity) at

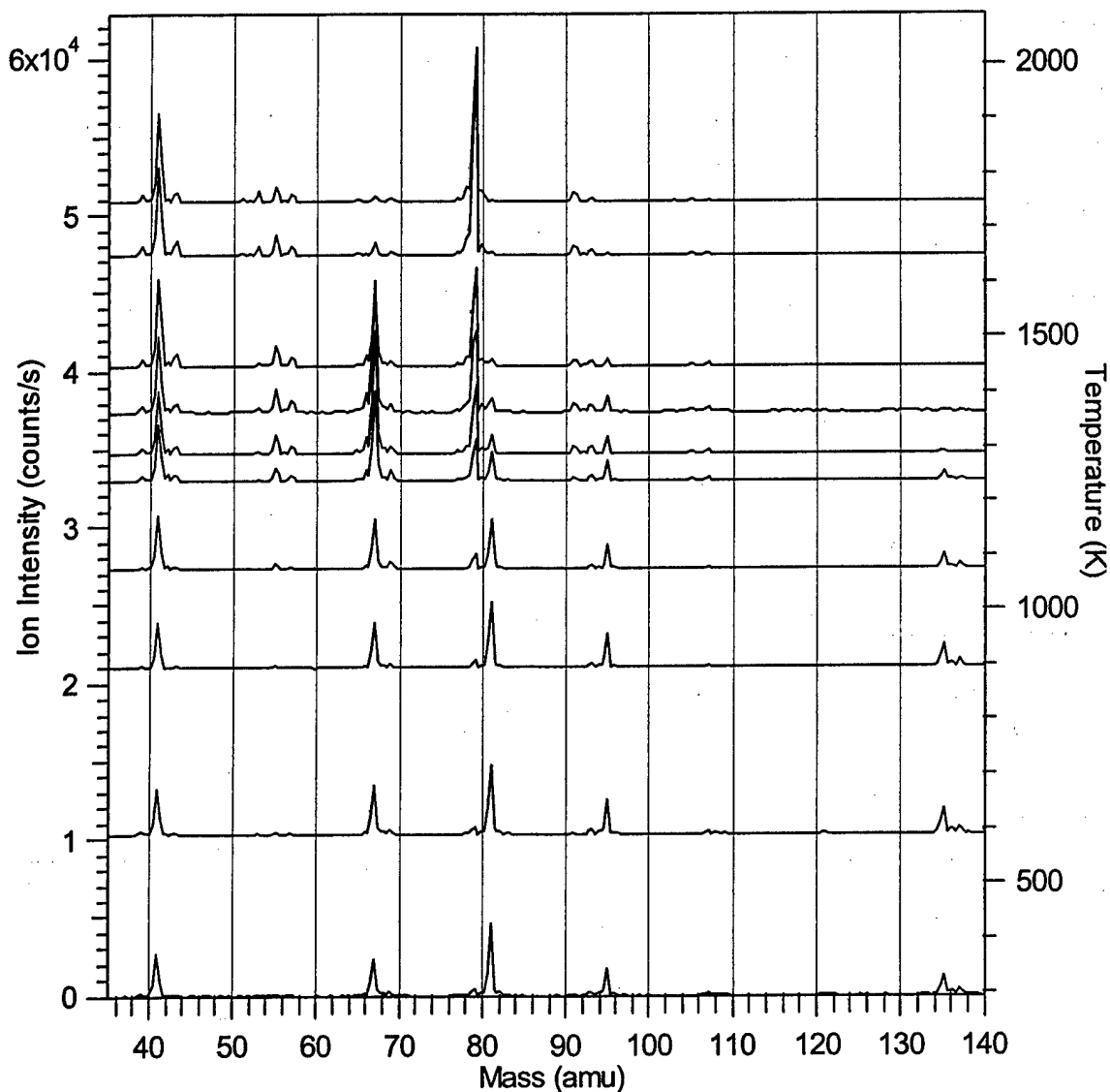


Figure 1. Pyrolysis mass spectra of JP-10 by Chemical Ionization

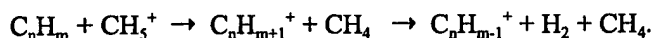
temperatures above 1300 K, where JP-10 is completely decomposed. The implication is that  $C_5H_7^+$  is produced both in CI-induced fragmentation of JP-10, and in CI of some pyrolysis product(s).

From fitting the temperature dependence of the disappearance of the JP-10 fingerprint peaks, it is straightforward to determine the breakdown v.s. temperature behavior of JP-10. In addition, however, we want to determine the product distribution as a function of temperature. For this purpose, we also studied pyrolysis mass spectra of various species that might be expected to be products, as well as species suggested by the major peaks in the high temperature JP-10 results. One major product peak is that at mass 67. This  $C_5H_7^+$  ion might result from proton transfer ionization of a  $C_5H_6$  pyrolysis product, or from protonation-induced fragmentation of a higher mass pyrolysis product. By far, the most stable  $C_5H_6$  compound is cyclopentadiene (CPD), and it is not difficult to imagine pathways by which this product might be generated from JP-10. The main peak in the low temperature CI spectrum of CPD is mass 67 ( $CPD + H^+$ ), with a smaller peak at 66 ( $CPD^+$ ), and several small peaks corresponding to adducts or fragments of adducts. The  $CPD^+$  peak probably results from direct electron impact ionization in our relatively low pressure CI source. The adduct peaks result from reactions with some of the hydrocarbon reagent cations generated in the CI process. For example, the peaks at 95 and 79 are attributed to ( $CPD + C_2H_5^+$ ) and ( $CPD + C_2H_5^+ - CH_4$ ), respectively, and 41 is attributed to ( $CPD + CH_5^+ - C_3H_6$ ). In the pyrolysis mass spectra of CPD, the mass 67 peak diminishes at high temperatures with concomitant growth in the mass 41 peak, indicating that CPD pyrolyzes above  $\sim 1500$  K on the experimental time scale, apparently losing  $C_2H_2$  to generate  $C_3H_4$ .  $C_3H_4$  is then ionized by proton transfer, yielding a mass 41 ion. Similar trends are observed for the mass 67 and 41 peaks in the pyrolysis mass spectra of JP-10 (Fig. 1), suggesting that CPD is the dominant carrier of the mass 67 signal, i.e., that CPD is a major JP-10 pyrolysis product. The EI mass spectra below provide further support for identifying CPD as a major JP-10 pyrolysis product.

One of the largest peaks in the JP-10 CI spectra at high T is at mass 79. This peak suggests a pyrolysis product with empirical formula  $C_6H_6$  ( $C_6H_7^+$  when protonated), and the only compounds with high enough stability to be likely products are benzene (BEN,  $\Delta H_f = 82.9$  kJ/mol) and methylene cyclopentadiene (MCPD,  $\Delta H_f = 223.8$  kJ/mol). Whatever this product is, it must be quite thermally stable, because the mass 79 peak remains substantial at the highest temperatures. The variable temperature CI mass spectra for benzene (BEN) shows an intense peak at mass 79, corresponding to protonated benzene, and that mass spectrum is nearly temperature-independent, showing signs of decomposition only at  $\sim 1800$ K. Such a mass spectrum is consistent with the persistence of the mass 79 peak in the high temperature JP-10 spectra, suggesting that benzene is a major high temperature pyrolysis product. We were unable to run spectra of MCPD for comparison, as this compound is not commercially available, however, its considerably higher  $\Delta H_f$  makes it quite unlikely that MCPD could be a JP-10 product, particularly at the higher temperatures. The CI peak at 79 could conceivably come from CI-induced fragmentation of some pyrolysis product of higher molecular weight, however, the EI data (below) rule out significant JP-10 breakdown into such products. The conclusion is that benzene is a major pyrolysis product, which is somewhat surprising because generation of benzene requires significant skeletal rearrangement. The lowest energy pathways to benzene from JP-10 probably correspond to production of  $C_4$  species, and mass peaks corresponding to  $C_4H_x$  appear over the same temperature range where benzene is first observed. At temperatures near 1200K, the dominant  $C_4$  peaks correspond to  $C_4H_7^+$  (55) and  $C_4H_9^+$  (57). If we assumed that these represent protonated molecular ions, that would imply that the product distribution contains one or more species with empirical formulae:  $C_4H_6$  and  $C_4H_8$  (plus  $C_4H_4$  at the highest temperatures). It is entirely possible, however, that the CI spectrum of the  $C_4H_x$  product(s) is complicated by  $H_2$  elimination from the nascent protonated molecular ion.

#### Electron Impact Studies of JP-10 pyrolysis

There are several drawbacks to use of methane CI in JP-10 pyrolysis studies. One, already noted, is that masses below  $\sim 40$  are inaccessible because of high background. In addition, the lack of standard CI spectra for comparison, can raise questions regarding spectral assignments. For example, the two main product ions,  $C_5H_7^+$  and  $C_6H_7^+$ , are highly stable ions, raising the possibility that they might originate from fragmentation of a higher mass neutral. In particular, it is not uncommon to lose  $H_2$  in proton transfer CI:



It is conceivable, therefore, that some or all of the  $C_5H_7^+$  CI signal might originate from  $C_5H_8$  rather than CPD, or that the  $C_6H_7^+$  CI signal might have contributions from products heavier than benzene. The fact that the temperature dependence of the CPD and benzene CI spectra is consistent with the JP-10 results, supports, but cannot prove the assignments.

To address these problems, we also studied JP-10 pyrolysis detecting products with electron impact ionization (EI). For typical hydrocarbons, EI results in extensive production of fragment ions, dependent on both the molecule and the electron energy. While the fragmentation attendant on EI can complicate spectral assignments, the great advantage is that the fragmentation patterns are not strongly dependent on the instrument, and libraries of EI mass spectra for thousands of compounds are available for comparison with unknown spectra.<sup>28</sup>

The JP-10 pyrolysis EI spectra are shown in Fig. 2. Consider the room temperature spectrum, i.e., the fingerprint spectrum for pure JP-10. The extensive fragmentation observed is consistent with the photoionization experiments of Federova et al.<sup>16,31</sup> who found that a variety of  $C_5$ ,  $C_6$ ,  $C_7$ ,  $C_8$ , and  $C_9$  fragment ions have appearance energies within 1 eV of the JP-10 ionization energy.

The EI spectra confirm the conclusions derived from the CI data. Most importantly, the JP-10 breakdown temperature dependence inferred from the EI and CI spectra is nearly identical. The EI data also corroborate the assignments of CPD and benzene as the only significant  $C_5$  and  $C_6$  pyrolysis products. In particular, the EI data definitively rule out any significant contributions to the pyrolysis product distribution from  $C_5H_x$  or  $C_6H_x$  ( $x > 6$ ) isomers. Consider  $C_5H_8$ . All 17 of the  $C_5H_8$  isomers listed in the NIST mass spectral database<sup>28</sup> give strong peaks at mass 67 and 68 under standard 70 eV EI conditions. In the EI spectra of JP-10 at high flow tube temperatures, where JP-10 is completely decomposed, the only peaks in the  $C_5$  mass range are at 65 and 66, eliminating the possibility that any of the  $C_5H_8$  isomers is present in significant concentration. Based on the analogous data for  $C_5H_{10}$ , and for  $C_6H_x$ ,  $x = 8, 10$ , we can conclude that the only significant  $C_5$  and  $C_6$  products are CPD and benzene, respectively.

This issue is important in light of the tentative conclusion from Hanson and co-workers that cyclopentene, rather than CPD, is produced in their JP-10 shock tube experiments. While it is possible that the difference reflects the higher temperatures and pressures in the shock experiments, we also note that their assignment was based on UV absorption spectroscopy. Assigning the broad UV spectrum observed for a mixture of hydrocarbons at high temperatures is a challenging problem. Unambiguous spectral assignment would require detailed simulations of the vibrational hot band structure for all the hydrocarbons that might be present. Because the high (and anharmonic) vibrational levels populated at high temperatures are poorly characterized, such detailed analysis is not generally feasible.

The EI spectra also allow us to probe low molecular weight pyrolysis products, although the analysis is complicated by EI-induced fragmentation of high molecular weight species into low mass ions. Note that even at room temperature, where JP-10 is the only hydrocarbon entering the ion source, there is substantial ion signal in the mass range below 50, mostly in the range around 40. It is clear that as the temperature is raised and JP-10 breaks down, the intensity of low mass ions increases substantially, implying that the increases result from EI of some pyrolysis product. Consider, for example, the temperature dependence of the mass 26 signal. This mass has negligible intensity at low temperatures, but is one of the major peaks in the high temperature EI spectrum. Before concluding that acetylene is a major pyrolysis product, however, we need to account for contributions to the high temperature 26 signal

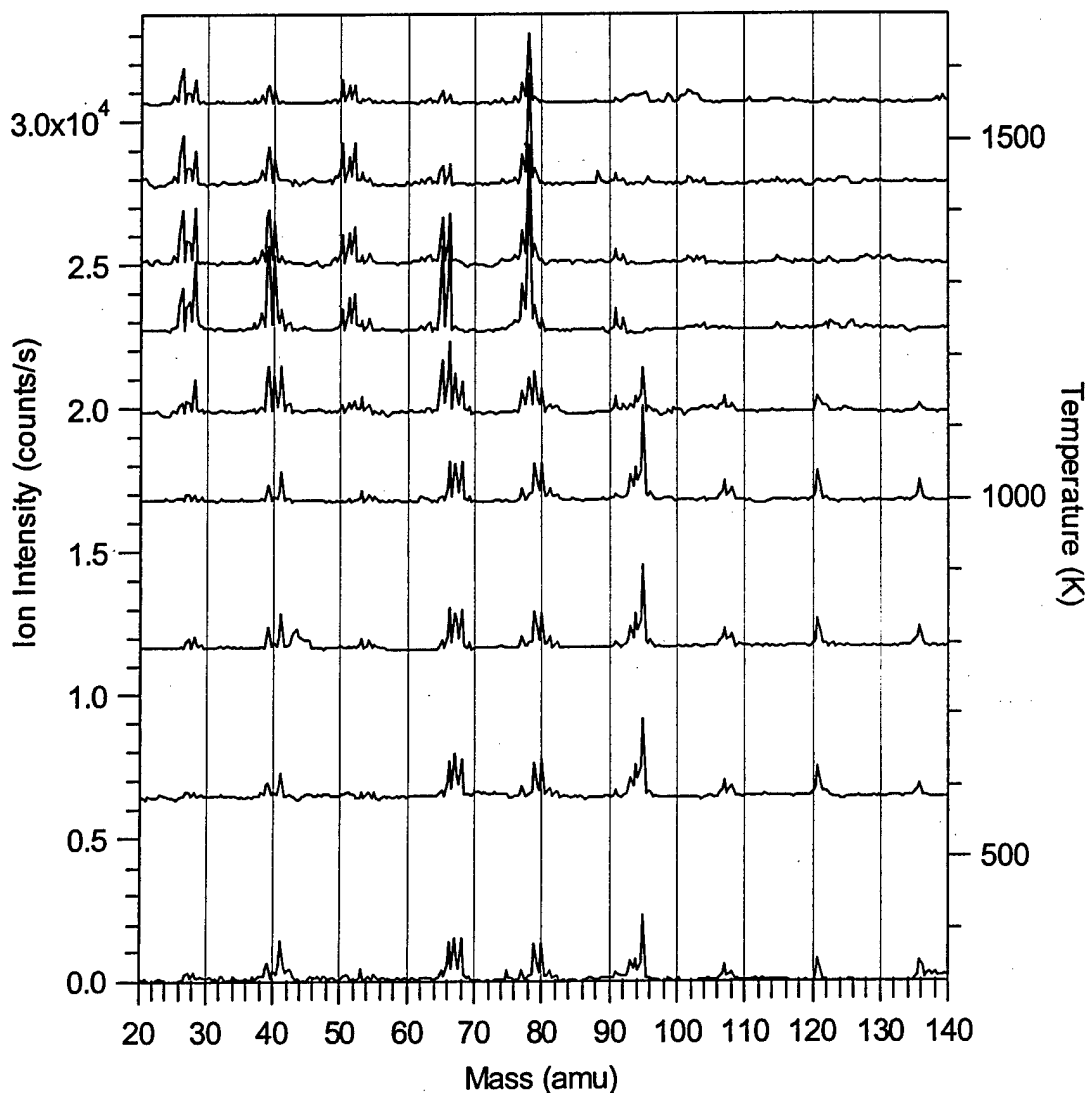


Figure 2. Pyrolysis mass spectra of JP-10 by electron impact (EI).

from EI-induced fragmentation of heavier pyrolysis products, such as CPD, benzene,  $C_4H_x$ , or  $C_3H_4$  – all identified in the high temperature CI spectra. Here, we take advantage of the existence of the extensive NIST library of EI mass spectra.<sup>28</sup> Note that in the high temperature JP-10 EI spectra, mass 26 is considerably more intense than 27. For CPD, benzene, and all common isomers of  $C_4H_x$  and  $C_3H_4$ , the EI fragmentation patterns have considerably higher intensity for 27 than 26. The implication is that these higher molecular weight pyrolysis products contribute only a small fraction of the mass 26 intensity, and therefore, that acetylene is an important high temperature JP-10 pyrolysis product. The acetylene peak begins to appear at ~1100 K, just above the temperature where JP-10 begins to decompose. Additional acetylene may result from secondary decomposition of CPD at high temperatures.

The other major low-mass peak at high temperatures is mass 28,  $C_2H_4^+$ . In this case, the important point to note is that 28 appears in the high temperature JP-10 spectra with much higher intensity than the neighboring mass 27 and 29 peaks. Standard EI mass spectra of likely  $C_3$ ,  $C_4$ ,  $C_5$ , and  $C_6$  species indicate that many such molecules do give significant mass 28 EI fragment peaks, however, they also tend to give strong peaks at mass 27 and/or mass 29.<sup>28</sup> We can, therefore, conclude that the

principle carrier of the 28 signal is EI of a pyrolysis product with molecular weight of 28, and this has to be  $C_2H_4$ . In order to account quantitatively for the contributions from higher molecular weight products to the 26 and 28 signals, it is necessary to fit the spectra, as described below.

The CI spectra have a considerable peak at mass 41 at high temperatures, assigned to protonation of a  $C_3H_4$  (propyne) pyrolysis product. The EI results, at first glance, appear to be inconsistent with this assignment. Note that the  $C_3$  region of the high temperature JP-10 spectra in Fig. 2 has a larger peak for mass 39 than mass 40. In contrast, the NIST EI spectrum of propyne has a large molecular mass peak (mass 40), and smaller peaks for mass 39 and other fragment ions. This apparent discrepancy is resolved when we consider that this mass range has contributions not only from ionization of  $C_3$  neutrals, but also from EI fragmentation of heavier neutral products. In particular, at the highest temperatures, where CPD is decomposed, benzene is the only major heavy product. In the NIST EI spectra of benzene there is no peak at mass 40 but a substantial peak at mass 39. Therefore, we can explain the mass 39:40 ratio observed for JP-10 at the highest temperatures, as follows. The mass 40 peak comes entirely from EI of propyne, while the mass 39 peak has contributions from both propyne and benzene. At somewhat lower temperatures, where CPD is a significant product, the NIST EI spectra indicates that EI fragmentation of CPD contributes to both mass 39 and mass 40, consistent with the observation that the 39:40 ratio changes substantially in this temperature range. These results confirm that  $C_3H_4$  is a major pyrolysis product of JP-10.

From the CI spectra, it was not possible to identify a single  $C_4H_x$  product responsible for the set of peaks appearing in the high temperature JP-10 spectrum (mass 55 with smaller peaks at 57 and 53). In EI of JP-10 at high temperatures, we observe intense peaks at mass 50, 51 and 52, with weaker peaks at mass 53 and 54. The peak at mass 51, along with some intensity at masses 50 and 52 is attributable to EI-induced fragmentation of benzene - CPD does not fragment significantly to  $C_4H_x^+$  in EI. After subtracting the benzene contributions, the balance of the intensity in this mass range (peaks at 50, 52, 53, and 54) must result from EI of some  $C_4$  product, or products. The spectra of a number of  $C_4$  species, such as various  $C_4H_8$  isomers, butadiene, 2-butyne and 1-but-3-yne are found in the NIST database.<sup>28</sup> All listed  $C_4H_8$  isomers can be eliminated, as they all give substantial peaks at masses 55 and 56, not observed in the JP-10 high temperature results. Butadiene, 2-butyne, and 1-but-3-yne have peaks at the right masses, but with intensity ratios different from that observed in the high temperature JP-10 results. We conclude that one or more  $C_4$  species are produced in JP-10 pyrolysis, but it is either a mixture, or a  $C_4$  isomer not in the database.

#### Data Fitting and JP-10 Breakdown

To extract quantitative JP-10 breakdown v.s. temperature results, the set of JP-10 pyrolysis mass spectra were fit, using a contracting grid, least-squares program developed for this purpose. The routine allows penalties to be assigned for non-physical fits (e.g., for negative residual peaks). The CI and EI spectra were fit independently, and the results subsequently merged, as described below. In both cases, the raw experimental spectra were first fit to generate stick spectra. These stick spectra were then fit as linear combinations of basis spectra, where the basis spectra were similarly generated stick spectra for known or suspected product species. Recall that the ion source is held at constant temperature and pressure, independent of flow tube temperature, and that there are sufficient collisions with buffer gas to equilibrate the gas entering the source prior to ionization. As a consequence, the basis spectrum for any given compound should be independent of flow tube temperature, at least up to the point where that compound begins to decompose. The EI spectra were fit over the mass range from 10 to 140, however, the CI spectra were fit only over the mass range from 40 to 140, as there is too much hydrocarbon background at lower masses. As noted above, no significant signal was observed in either EI or CI in the mass range from 140 to 300.

The basis spectra used in the fits were generated as follows. For EI, where a library of standard spectra is available,<sup>28</sup> the basis spectra were simply these standard spectra for the various possible pyrolysis products identified from the combination of EI and CI results, discussed above. EI basis spectra were included for  $C_2H_2$ ,  $C_2H_4$ , propyne, CPD, benzene, and JP-10. No standard spectrum is available for JP-10 itself, and we simply used our spectrum taken for the room temperature flow tube. For CI, no

standard spectra are available. For JP-10 and the two major high molecular weight pyrolysis products, CPD and BEN, we simply used our experimental CI spectra measured for the room temperature flow tube. It is clear from both CI and EI data, that  $C_3H_4$  (propyne) is a significant pyrolysis product, detected as  $C_3H_5^+$  (mass 41) in CI. To represent this product, a basis spectrum consisting of a single peak at mass 41 was used. These four basis spectra (JP-10, BEN, CPD, propyne) account for most of the intensity observed in the CI spectra, and the same species, with the addition of  $C_2H_2$  and  $C_2H_4$ , also account for most of the EI spectral intensity.

In addition, however, both EI and CI results indicate the presence of at least three additional minor products, more clearly seen in CI, where there is less fragmentation. There is clearly one or more  $C_4H_x$  products, and as described above, neither the CI nor EI peak patterns allows clear identification. In the case of CI, the basis spectrum for  $C_4H_x$  was generated simply by taking the mass 50 to 56 range from the experimental high temperature JP-10 CI spectra. For EI, we generated a synthetic  $C_4H_x$  spectrum from the standard spectra for butadiene, 2-butyne, 2-butene, and 1-but-3-yne, adjusting the contributions of each component to approximately match the experimental high temperature JP-10 spectrum in the mass 50 to 56 range, after first subtracting the contribution from dissociative ionization of benzene. Note: we do not claim any significance to the particular combination of standard spectra used in this composite – it is simply a convenient way to generate a " $C_4H_x$ " spectrum.

Both EI and CI at high temperature also have a pair of weak peaks indicating one or more minor  $C_7H_x$  product(s). For CI, we included a basis spectrum consisting of these  $C_7H_x$  peaks taken from the high temperature spectra. For EI these peaks are so weak that they were simply allowed to fall into the category of "unfit residuals". The CI spectra at high temperatures also have weak groups corresponding to  $C_8H_x$  and  $C_{10}H_x$ . Because these are so weak, they were allowed to fall into the unfit residuals.

The CI fitting results are given in Fig. 3, and the EI fitting results are given in Fig. 4. Note that these figures give the contribution of each basis spectrum to the total ion signal at each temperature. Analysis to extract the desired neutral concentrations is discussed below. Note also that the sum of the

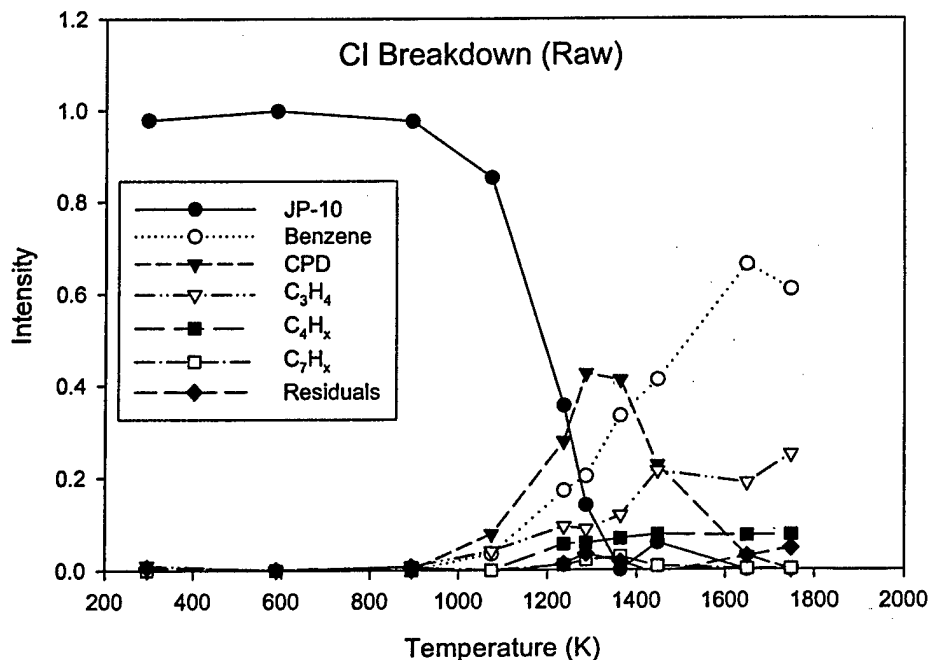


Figure 3. CI breakdown of JP-10

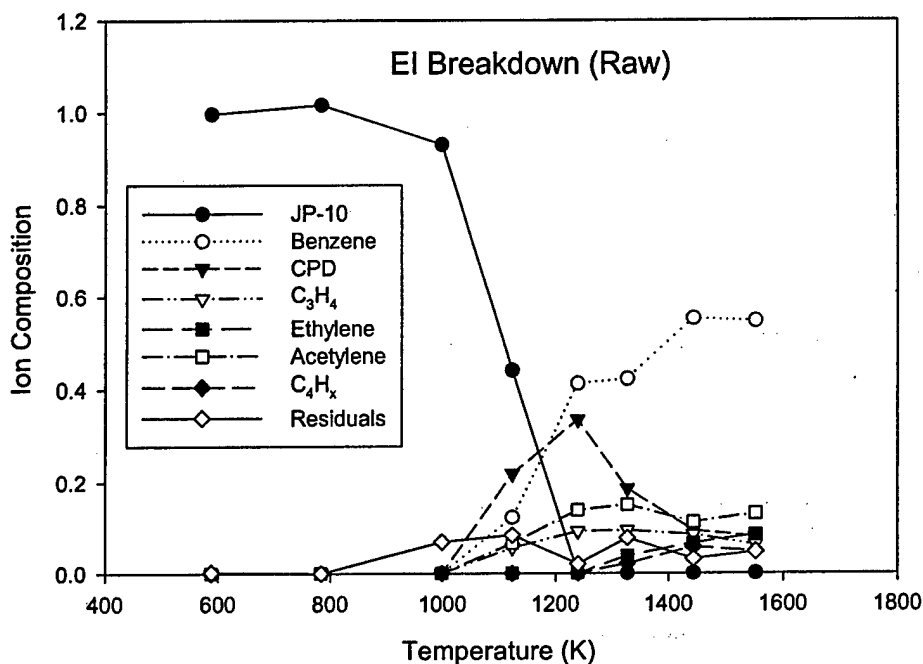


Figure 4. EI breakdown of JP-10

contributions at each temperature is normalized to unity in each figure, thus because different numbers of components are included in the CI and EI fits, the normalizations are somewhat different. The two data sets are merged below. In general, the EI and CI data are in good agreement. JP-10 begins to decompose between 900K and 1000K, and is completely decomposed by ~1350K. Initially, CPD is a major product, but it is replaced by other products at higher temperatures. The major high temperature products are benzene, propyne, C<sub>2</sub>H<sub>2</sub>, C<sub>2</sub>H<sub>4</sub>, with smaller amounts of C<sub>4</sub>H<sub>x</sub> and C<sub>7</sub>H<sub>x</sub>. The data series labeled "Unfit Residuals" in the CI results mostly consists of a variety of minor C<sub>8</sub> and C<sub>10</sub> species not included in the fits, and the fact that the residuals are so small is a good indication of the fit quality. The "Unfit residuals" is larger for EI, for several reasons. The EI residuals at high temperatures partly reflect the fact that the EI fits do not include a basis spectrum for C<sub>7</sub>H<sub>x</sub>, which was separately broken out in the CI fits. The major reason for the higher EI residuals, especially at low temperatures, is that the EI spectra for individual compounds are not completely independent of flow tube temperature, contrary to what is assumed in the fitting process. This effect can be seen by noting that the JP-10 EI spectrum changes slowly with temperature in the range below 900 K, where JP-10 has not started to decompose. This dependence on flow tube temperature probably results from the lower ion source pressure under EI conditions, which apparently is insufficient to equilibrate the analyte molecules at the ion source temperature prior to ionization. Because fitting under these conditions is less reliable, the analysis below will rely mostly on the CI results. The EI results are used only to determine the concentrations of low molecular weight products, and to confirm the identification of the CPD and benzene products, as discussed above.

Figs. 3 and 4 show compositions as a fraction of the *ion* signal in the CI and EI mass spectra. To convert these to the fractional composition of the *neutral* species exiting the flow tube, it is necessary to correct for variations in ionization efficiency for the different compounds. Note that this correction does not affect the temperature dependence derived for any given compound (e.g. JP-10), but only the relative contribution of the different compounds to the product distribution.

For CI, ionization is primarily by proton transfer in the CI source, and the relative efficiency is determined by the product of the collision cross section and the proton transfer efficiency *per* collision.

Fortunately, the literature is full of examples of proton transfer rate constants<sup>32</sup>, and in every case where the proton transfer reaction is exothermic, the reaction occurs on every collision. In our case, the dominant CI reaction is:  $\text{CH}_5^+ + \text{M} \rightarrow \text{MH}^+ + \text{CH}_4$ , thus the reaction exothermicity depends on the difference in proton affinity between M and  $\text{CH}_4$ ,  $\Delta\text{PA}(\text{CH}_4)$ .  $\text{CH}_4$  is used in CI precisely because it has an unusually low proton affinity. As a consequence, the proton transfer reactions are highly exothermic for all species of interest, and this correction factor is, therefore, unity for all species.

Under the thermal conditions in the CI source, the collision cross section is accurately given by the capture cross section ( $\sigma_{\text{cap}}$ ),<sup>33</sup> which can be calculated knowing only the polarizabilities and dipole moments of the analyte molecules. These are known for some analyte molecules, and the rest can be easily calculated using quantum chemistry methods. Quantum chemistry calculations at the B3LYP/6-31G\* level were performed using GAUSSIAN 98.<sup>29</sup> In cases where identity of the product species is not clear ( $\text{C}_4\text{H}_x$ ,  $\text{C}_7\text{H}_x$ , ...), the values used were averages for several representative molecules. The relative capture cross section for the various products,  $\sigma_{\text{cap}}(\text{product})/\sigma_{\text{cap}}(\text{JP-10})$ , ranges from  $\sim 0.73$  (propyne) to  $\sim 1.1$  ( $\text{C}_{10}\text{H}_x$ ).

The EI data also need to be corrected for the electron impact ionization efficiency, i.e., for variation in the electron impact ionization cross section from molecule to molecule. The EI cross sections are not known for most of the molecules of interest, but a number of studies have been reported aimed at formulating rules for estimating electron impact ionization cross sections in terms of polarizabilities or other simply determined molecular parameters. For example, Flaim and Ownby<sup>34</sup> and Nishimura and Tawara<sup>35</sup> report linear dependence of the ionization cross section on the number of electrons in the molecule. The linear scaling appears to be reasonably good (within 10%) except for species like He and Ne, with unusually compact electron clouds. Given that all the molecules of interest for our purposes are hydrocarbons, i.e., all the same class of molecule, linear scaling of ionization efficiency with electron count is adequate for correcting our EI data.

As noted, we feel that the product distribution inferred from the CI data is more reliable because

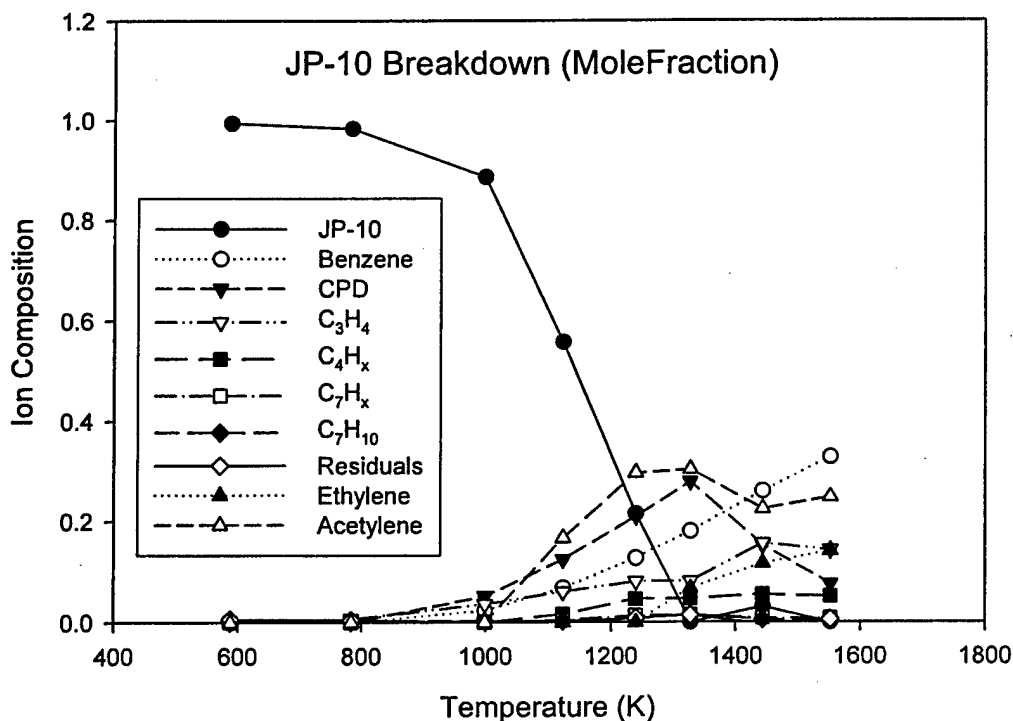


Figure 5. Breakdown distribution for JP-10 as neutral mole fraction

the higher source pressure appears to thermalize the analyte molecules prior to detection, as is assumed in the fitting process. In addition, CI results in little fragmentation of most of the product species, simplifying the fitting process. We will, therefore, use the CI product distribution, simply adding the  $C_2H_2$  and  $C_2H_4$  contributions deduced from EI. Figure 5 shows the combined results, plotted as mole fraction.

JP-10 begins to decompose at around 1000K, and is completely decomposed by ~1350K. At low temperature CPD is the main product but it is unstable at high temperature and begins to decompose at around 1350K. The major high temperature products are benzene, propyne,  $C_4H_x$ , acetylene, ethylene and a variety of minor  $C_8$  and  $C_{10}$  species, grouped under "Unfit residuals" in the figure.

#### Comparison of Experimental and Computational Results

Equilibrium calculations were performed using the Cantera program and a mechanism based on merging the species in the JP-10 mechanism suggested by Williams et al.<sup>24,36</sup> and a mechanism developed by Violi et al. for PAH formation. The calculation was run at the experimental temperatures and the pressures were specified to match the mid-point pressures of the flow tube reactor. The initial mole fraction of JP-10 was 1.0. The results are compared with the experimental product distribution in Table II. Not surprisingly, given the millisecond experimental time scale, the equilibrium calculations are in very poor agreement with the experimental results. More interesting, we note that the equilibrium product distribution has essentially no benzene or CPD, which are the major products experimentally, particularly at intermediate temperatures. The equilibrium calculation also predicts a substantial branching to  $CH_4$ , which is not observed experimentally. The experiments were not able to measure  $H_2$ , therefore we cannot comment on the high  $H_2$  concentration predicted.

As noted in the introduction, the mechanism for JP-10 decomposition is not well understood, and one aim of our study is to provide feedback for developing an improved mechanism. Toward this end Violi and Marsh are engaged in a theoretical study of JP-10 decomposition using a combination of ab initio calculations to identify decomposition pathways, and kinetic modeling to refine the mechanism. For comparison purposes they provided us with a preliminary calculation performed using the CHEMKIN II/SENKIN programs.<sup>37,38</sup> The mechanism used in these calculations included reactions from the reduced JP-10 mechanism of Williams et al.,<sup>1</sup> combined with a mechanism developed for a JP-8 surrogate fuel by Violi et al.<sup>39</sup> In their calculation, the pressure was set to 2 Torr of neat JP-10, and product distributions were calculated for 20 and 100 msec time scales (compared to ~7% JP-10 in rare gas and 2-10 msec reaction time in the experiments). The calculated breakdown temperature dependence is shifted ~150 K to higher temperature relative to the experiments, and presumably, if the calculations had been done for the shorter experimental time scale, the shift would be larger. The calculated product distribution is in poor agreement with the experiments. The calculated distribution is dominated by  $C_2$  products even at the onset of JP-10 decomposition. No CPD is predicted at any temperature, and the benzene mole fraction is never above ~0.1, compared to 0.33 experimentally. The bias toward  $C_2$  products comes from the reduced JP-10 mechanism, where the lowest energy JP-10 pyrolysis reaction is taken as  $C_{10}H_{16} \rightarrow C_2H_2 + 2C_2H_4 + C_4H_6$ . The absence of CPD as a predicted product reflects absence of reactions generating  $C_5H_6$  in the mechanism. The discrepancies point out the need for a mechanism incorporating chemistry that can account for the observed  $C_3$  and  $C_6$  products, and developing this chemistry is the focus of Violi and Marsh's on-going work.

Table I. Flow tube properties under chemical ionization (CI) and electron impact ionization (EI) conditions.

T (K)	P <sub>midpoint</sub> (Pa)	Density (moles/m <sup>3</sup> )	Velocity (m/sec)	Residence time (msec)
CI Conditions				
298	274	0.11	10.7	9.35
898	336	0.05	26.3	3.81
1498	389	0.03	37.9	2.64
EI Conditions				
298	181	0.07	16.2	6.18
898	254	0.03	34.9	2.87
1498	309	0.02	47.7	2.10

Table II. Comparison of experimental and calculated equilibrium product distribution

T (K)	EXPERIMENTAL							
	JP-10	BEN	CPD	C <sub>3</sub> H <sub>4</sub>	C <sub>2</sub> H <sub>2</sub>	C <sub>2</sub> H <sub>4</sub>	C <sub>4</sub> H <sub>x</sub>	Other
588.3	1.000	0.000	0.000	0.000	0.000	0.000	0.000	0.000
783.6	0.988	0.000	0.000	0.007	0.000	0.000	0.000	0.005
998.7	0.886	0.023	0.051	0.036	0.000	0.000	0.000	0.004
1123.5	0.558	0.068	0.124	0.061	0.167	0.000	0.016	0.007
1239.8	0.217	0.127	0.210	0.082	0.298	0.000	0.047	0.020
1327.4	0.000	0.182	0.281	0.082	0.307	0.069	0.048	0.030
1443.4	0.029	0.258	0.151	0.155	0.224	0.115	0.054	0.014
1552.1	0.000	0.329	0.076	0.143	0.249	0.142	0.051	0.010
T(K)	EQUILIBRIUM							
	JP-10	BEN	CPD	C <sub>3</sub> H <sub>4</sub>	C <sub>2</sub> H <sub>2</sub>	C <sub>2</sub> H <sub>4</sub>	H <sub>2</sub>	CH <sub>4</sub>
588.3	0.000	0.000	0.000	0.000	0.000	0.000	0.030	0.837
783.6	0.000	0.000	0.000	0.000	0.000	0.000	0.396	0.479
998.7	0.000	0.000	0.000	0.000	0.000	0.000	0.822	0.062
1123.5	0.000	0.000	0.000	0.000	0.002	0.000	0.866	0.018
1239.8	0.000	0.000	0.000	0.000	0.015	0.000	0.867	0.006
1327.4	0.000	0.000	0.000	0.000	0.051	0.000	0.840	0.003
1443.4	0.000	0.000	0.000	0.000	0.195	0.000	0.723	0.001
1552.1	0.000	0.000	0.000	0.000	0.448	0.000	0.498	0.000

## Nanocatalysis Section:

### I. Introduction:

An important problem in use of complex liquid hydrocarbon fuels for high speed propulsion applications, is getting ignition delays short enough, and combustion rates fast enough. Example engines where combustion speed/ignition delay is a significant issue are pulse detonation engines, ramjets, and scramjets. In the case of the Pulse Detonation Engine (PDE), it is essential that the combustion chemistry be fast enough to feed energy back into the detonation shock, ensuring that the detonation propagates. It is also important that detonability be maintained with no added oxygen, and over a wide range of altitudes and flight speeds. One approach is to add fuel additives that break down to generate radicals at low temperatures, thus starting the combustion chain reaction, however such additives can lower energy density and/or decrease the storability of the fuel. We are proposing to examine prospects for a special type of fuel additive – nanoparticles that will act both as a catalyst to accelerate hydrocarbon fuel ignition, and as a high energy density fuel to increase net energy density.

The catalyst particles will be nanoparticles with an inner cores of a combustible metal or other high energy density material, surrounded by a shell of, or containing, a catalyst material. The outer shell is intended to speed ignition and increase combustion rates by catalyzing combustion of the hydrocarbon fuel. Once hydrocarbon combustion is well initiated, temperatures would reach the point where the metal core of the particle combusts, releasing the energy content of the metal core. For some metal/catalyst combinations, there may also be a thermite-type solid state reaction that contributes to heat release, and increases combustion efficiency of the metal core.

In the balance of the proposal text, I will first elaborate on the idea, using some calculations to illustrate the potential, and estimating some parameters of interest for optimizing the desired effects. These calculations are followed by preliminary data showing that a significant catalytic effect is possible. Finally, I will discuss what we propose to do in furthering the research and application to Navy problems. Because of the nature of the work, collaborations of chemists (us) with engineers will be necessary. One ONR PI (Sumanta Acharya) has already gotten promising results with  $\text{CeO}_2$  nanopowder we provided to him. Other PIs have indicated an interest in examining the effects of catalyst addition in different combustor configurations.

### II. Elaboration of the concept

Combustion catalysts are common for industrial power generation. In such applications, the catalyst is generally immobilized on a support, and the reactants are passed through a catalyst bed where combustion is initiated. The catalyst increases combustion efficiency, and allows operation at lower temperatures, reducing  $\text{NO}_x$  formation. Flow rates are relatively large, allowing long contact times with the catalyst. For air-breathing propulsion applications, it generally is not feasible to pass the fuel-air mix through a catalyst bed, as the flow resistance is too high. In addition, for PDE, ramjet and scramjet applications, the combustion times need to be very fast.

The idea being explored here is pre-mixing the catalyst with the fuel-air mixture, and allowing it to flow through the combustor. In order that the catalyst significantly accelerates the gas-phase chemistry, the catalyst surface area must be large, and well dispersed in the fuel/air mix. Both requirements can be met by using nanoscale catalyst particles, with volume loadings in the 10% range. Such high volume loadings of a pure catalyst would be quite undesirable from the energy density perspective, as combustion catalysts are typically either metal oxides, or precious metals, neither of which contributes to the energy density. The loss of energy density can be overcome by

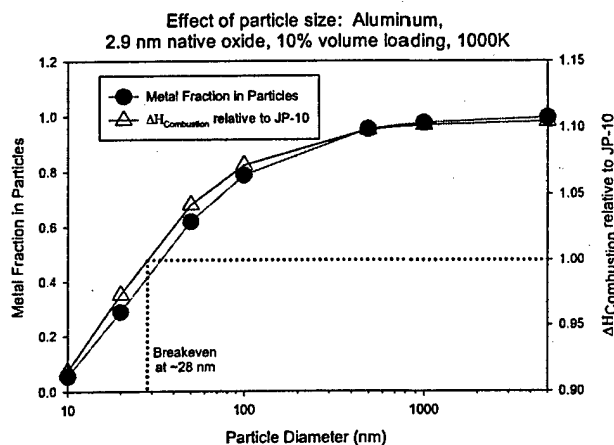
Fuel	Density kg/L	$\Delta H_{\text{comb}}$ kJ/Mol	$\Delta H_{\text{comb}}$ kJ/kg	$\Delta H_{\text{comb}}$ kJ/L
Al	2.69	810	30022	81003
Mg	1.74	550	22633	39382
B	2.34	627.5	58048	135832
JP-10	0.94	5709.28	41980	39461

using core/shell catalyst particles, where the shell is catalyst material, while the core, making up the bulk of the particle mass, is an energetic material, such as aluminum, boron, or magnesium.

The table compares densities and molar, gravimetric, and volumetric heats of combustion ( $\Delta H_{\text{comb}}$ ) for three metals of interest as energetic core materials. The metal properties are compared with those for JP-10, which is taken as the benchmark. For most Navy applications, the volumetric energy density is most important, thus Al and B represent significant improvements over JP-10, so that adding nanoparticles of those materials will increase net energy density. Our initial experiments focused on aluminum, because well characterized nanoparticles are readily available, however, boron may also be an attractive possibility.

#### A. Effects of particle size:

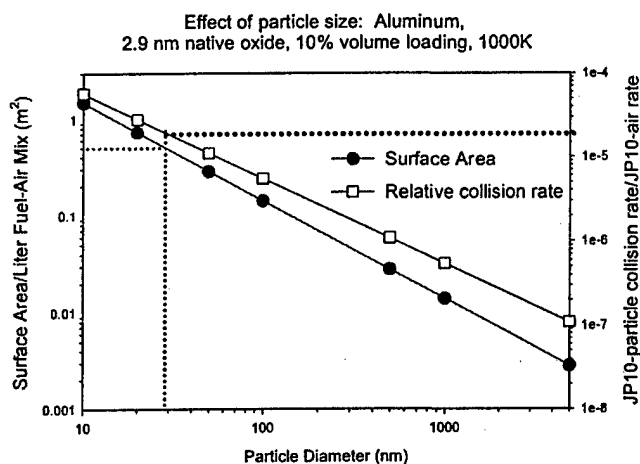
Several figures of merit are reviewed in the following figures. Aluminum particles have a native  $\text{Al}_2\text{O}_3$  oxide layer about 3 nm thick, that protects them from further oxidation. The figure at right shows the variation in metal fraction with particle size. Note that for particles larger than  $\sim 30$  nm, more than half the particle mass is aluminum. The figure also compares the volumetric  $\Delta H_{\text{comb}}$  for JP-10 loaded with 10% by volume of nanoparticles, relative to that for pure JP-10. Because aluminum's  $\Delta H_{\text{comb}}$  is about twice that of JP-10, the aggregate  $\Delta H_{\text{comb}}$  is greater than that of pure JP-10 for any particle size greater than  $\sim 28$  nm.



In the next figure, results are shown for the nano-particle laden fuel (10 volume %), dispersed as a stoichiometric fuel-air mixture at 1000 K and 1 atm total pressure. One curve shows the particle surface area per liter of fuel-air mix. Note that for particles in the 50 nm range, the surface area is  $1 \text{ m}^2$  per liter of fuel-air mix. The second curve shows perhaps the most important figure of merit from the perspective of possibly catalytic activity. This is the relative rates of JP-10 collisions with particles surfaces, compared to the gas-phase collision rate. For 50 nm particles, there will be about one JP-10 surface collision for every  $10^5$  gas-phase collisions, or  $\sim 10^{18}$ /sec/liter of fuel-air mix. This may seem to indicate that catalytic effects will be negligible, however, it should be remembered that catalytic rates can be many orders of magnitude greater than uncatalyzed rates, particularly for temperatures where the homogeneous rates are slow, as in ignition. As will be shown below, catalytic effects are, indeed, significant.

#### B. Catalytic Materials of Interest

One important property of the catalyst particles that can be adjusted to optimize fuel performance, is the nature of the catalytic coating applied to the particle surface. As noted, the aluminum particles are coated with a passivating native oxide layer. Pure alumina is a poor catalyst, thus for most applications, it will be desirable to dope the alumina layer or coat the particles with a thin layer of more active catalyst. A wide variety of materials have been investigated as combustion catalysts,<sup>40-46</sup> ranging from transition metals and their oxides, noble metals and compounds thereof,<sup>47-54</sup> alkaline earth compounds, and rare earth compounds.<sup>49,51,55-57</sup> In many cases mixtures are used. The requirements for a catalyst in the proposed



application are different from those in catalysts for power generation. There, the primary goal is to lower flame temperature, so as to limit  $\text{NO}_x$  formation. High porosity and long term stability are also critical. For the purposes of the proposed propulsion catalyst/fuel, we are looking for high combustion rates, high flame temperatures, and ability to coat onto the fuel nanoparticles easily. In addition, the catalyst will be used in a single-pass mode. This means that we don't need to worry about catalyst stability, however, we do need to minimize use of expensive materials. We initially plan to focus our efforts on several classes of catalyst materials. The most promising are oxides, including rare earth oxides and transition metal oxides. Example systems are  $\text{CeO}_2$ ,  $\text{NiO}_x$ ,  $\text{PdO}$ , and mixed rare earth-transition metal oxides. Example data for  $\text{CeO}_2$  will be discussed below. In these materials, the oxygen is bound less strongly than in highly stable oxides, such as  $\text{Al}_2\text{O}_3$  or  $\text{MgO}$ . It is possible for such materials to act as a O-atom source, converting impinging hydrocarbon molecules to partially oxidized species, initiating the cascade of elementary reactions that ultimately converts hydrocarbons to  $\text{CO}_2$  and water. To complete the catalytic cycle, the oxide surface is regenerated by reaction with  $\text{O}_2$  in the fuel-air stream. Depending on the specific rare earth or mixture of rare earths used, the catalyst may also assist in activating (i.e., breaking) CH or CC bonds in the hydrocarbon reactant.

For many oxide catalysts, there is the additional possibility of a thermite-type reaction once the temperature is high enough to disrupt the passivating  $\text{Al}_2\text{O}_3$  layer. For example:

1.  $2 \text{Al} + \text{Fe}_2\text{O}_3 \rightarrow 2\text{Fe} + \text{Al}_2\text{O}_3$   $\Delta H = -865 \text{ kJ/mol}$
2.  $2 \text{Al} + 1.5 \text{TiO}_2 \rightarrow 1.5 \text{Ti} + \text{Al}_2\text{O}_3$   $\Delta H = -283 \text{ kJ/mol}$
3.  $2 \text{Al} + 3 \text{TiO}_2 \rightarrow 3 \text{TiO} + \text{Al}_2\text{O}_3$   $\Delta H = -502 \text{ kJ/mol}$
4.  $2 \text{Al} + 1.5 \text{CeO}_2 \rightarrow 1.5 \text{Ce} + \text{Al}_2\text{O}_3$   $\Delta H = \sim -55 \text{ kJ/mol}$

All these reactions are exothermic. Data needed to estimate the energetics for conversion of  $\text{CeO}_2$  to a lower oxidation state oxide (analogous to reaction 3) are not available, but it is likely that such a reaction exists, with higher exoergicity than reaction 4 (c.f. reactions 2 and 3). The importance of these reactions is that they may increase the efficiency with which the aluminum core combusts. For systems with exothermic thermite type reactions, the overall process is as follows:

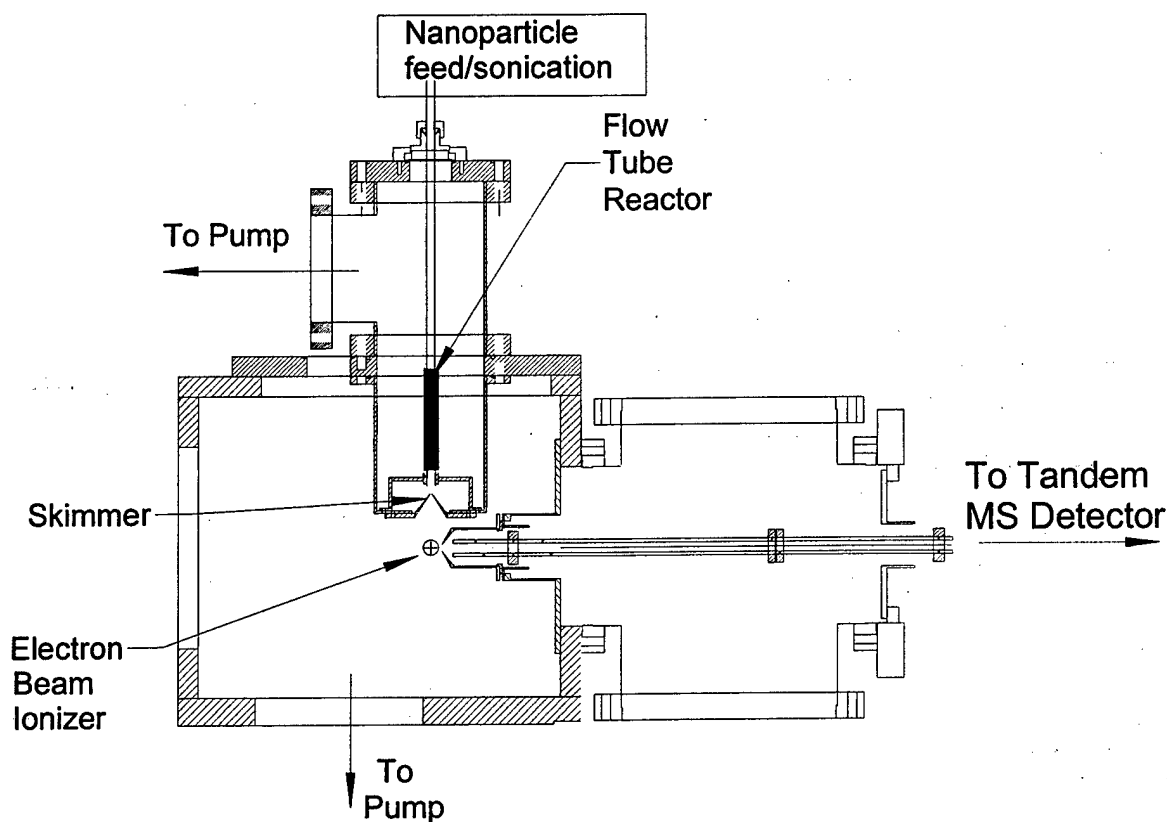
**Stage One:** The catalyst coating catalyzes ignition and combustion of the hydrocarbon fuel.

**Stage Two:** Once hydrocarbon combustion heats the particles, the thermite reaction occurs. Depending on the energetics, and relative amounts of core and shell material, the energy release may vaporize a significant fraction of the metal core.

**Stage Three:** The hot partially vaporized metal core material burns.

### Experimental Setup

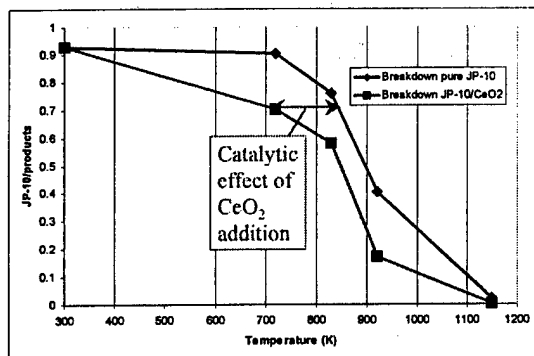
The catalyst characterization work will use our existing flow tube reactor/mass spectrometer system, constructed with ONR support. The current modification of the instrument is shown in the figure. The tandem guided-beam mass spectrometer has been described in detail previously,<sup>26,27,58,59</sup> and I will describe only on the modifications carried out for the proposed experiments. The main modifications were changing to a vertical flow tube geometry, adding an additional stage of differential pumping to allow higher flow tube pressure, adding an external electron beam ionizer, and developing a mechanism for controlled feeding of nanoparticles into the gas flow. This modification is fully operational, and initial results will be discussed below. We continue to refine the nano-powder feed mechanism, aiming for smoother feed rates.



In these experiments, the fuel of interest (e.g. JP-10) is premixed with a carrier gas, which might be an inert gas, oxygen, or air, then flowed through the vertical flow tube at a total pressure of  $\sim 20$  Torr. The mass flow rate in the current tube is  $\sim 20$  times greater than the earlier version of the flow tube reactor. The flow tube is heated to a desired temperature, ranging up to  $\sim 2000$ K, and the composition of the gas exiting the tube is measured by mass spectrometry. By taking mass spectra as a function of temperature, we are able to measure the breakdown behavior of the fuel. See Fig. 2 above, for an example. To examine catalytic effects, the experiment is repeated with identical flow parameters, but with nano-powder being fed into the top of the flow tube. The differences between the mass spectra with and without catalyst addition are attributable to reactions on the surface of the catalyst. We synthesized and characterized with electron microscopy, a number of different sizes of  $\text{CeO}_2$  particles, and sample results are presented here for  $\text{CeO}_2$  with  $\sim 20$  nm grain size, in micron size aggregates. The effect on overall breakdown behavior is shown in the figure at right, which compares the breakdown of JP-10 with and without  $\text{CeO}_2$  addition. Note that the breakdown curve shifts about  $150$ K to lower temperatures, indicating that  $\text{CeO}_2$  is facilitating the disappearance of JP-10.

In addition to the shift in breakdown kinetics, there are also large changes in the decomposition product distribution. Note that for JP-10/ $\text{O}_2$  mixtures, without catalyst, we observe that:

1. There is no shift in the onset temperature of JP-10 decomposition, indicating that the limiting factor is pyrolysis of JP-10, rather than reaction with  $\text{O}_2$

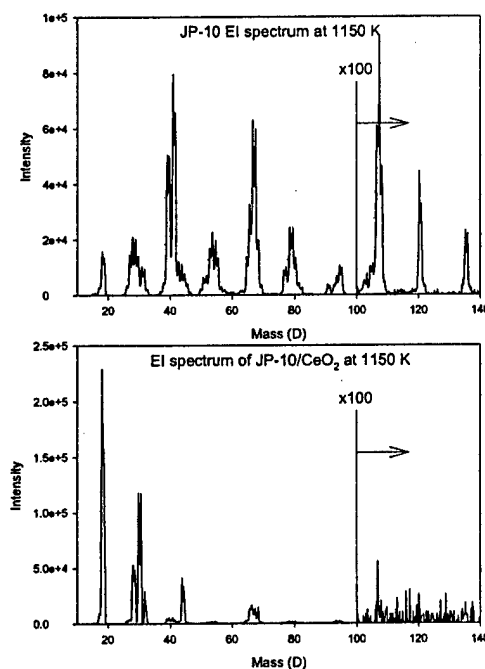


2. Once pyrolysis gets started, the kinetics are slightly speeded up by  $O_2$ , indicating that the JP-10 pyrolysis products can react with  $O_2$
3. For pure JP-10, the pyrolysis products are hydrocarbons such as benzene, propyne, ethylene, acetylene, and cyclopentadiene. When sub-stoichiometric concentrations of  $O_2$  are present, no products with molecular weight less than 300 are observed, indicating that the product distribution has shifted to some sort of polymer product (i.e., soot precursors).

For JP-10 with no  $O_2$ , but with added  $CeO_2$ , the product distribution is dominated by oxidation products, as shown by the figure at right. The top spectrum is a electron impact (EI) mass spectrum of JP-10 after passing through the flow tube at 1150K. Note that the high mass peaks indicative of JP-10 are small (scaled by 100 to be visible), indicating that most of the JP-10 has decomposed at this temperature. The products are a series of hydrocarbons, including cyclopentadiene (mass 66) benzene (78), propyne (40),  $C_2$  hydrocarbons (masses 26, 28, 30) and EI-induced fragments thereof.

The lower spectrum is for an identical flow, but with  $CeO_2$  added. Note that the high mass peaks are completely gone, indicating that the JP-10 decomposition is promoted by the catalyst. Note also that the only products are masses 18 (water), 28 (CO), 30 ( $H_2CO$ ), 44 ( $CO_2$ ), and 66 (cyclopentadiene?). This change in product distribution proves that one effects of the  $CeO_2$  is to act as an oxygen source, because in this experiment, there was no other added oxygen. In a real combustion situation, the  $CeO_2$  surface would be replenished by reaction with atmospheric  $O_2$ , completing the catalytic cycle.

These results demonstrate that collisions with catalyst surfaces can significantly increase decomposition/oxidation rates. Under the conditions of this experiment, each JP-10 molecule makes only a few collisions with a  $CeO_2$  surface, leading to complete conversion to low molecular weight oxidized products. In the experiments, mentioned above, where JP-10/ $O_2$  mixtures were passed through the flow tube with no catalyst, no oxygen-related chemistry is apparent that this temperature, even though the average number of JP-10 -  $O_2$  collisions was  $\sim 10,000$  under the conditions used. It should be recognized that  $CeO_2$  was chosen more for convenient nanoparticle synthesis, and that the combustion catalyst literature suggests that substantial further gains are possible with better catalysts.



References

- 1 S. C. Li, B. Varatharajan, and F. A. Williams, *AIAA J.* **39**, 2351 (2001).
- 2 N. K. Smith and W. D. Good, *Aiaa J.* **17** (8), 905 (1979).
- 3 J. E. Peters and A. M. Mellor, *J. Energy* **7** (1), 95 (1982).
- 4 R. Atkinson, S. M. Aschmann, and W. P. L. Carter, *Int. J. Chem. Kinet.* **15** (1), 37 (1983).
- 5 G. W. Burdette, US Patent No. 4410749 (1983).
- 6 G. A. Szekely, Jr. and G. M. Faeth, *Combust. Flame* **49** (1-3), 255 (1983).
- 7 P. Antaki and F. A. Williams, *Combust. Flame* **67** (1), 1 (1987).
- 8 L. C. Clausen, T. X. Li, and C. K. Law, *J. Propul. Power* **4** (3), 217 (1988).
- 9 F. Takahashi, F. L. Dryer, and F. A. Williams, *Symp. (Int.) Combust., [Proc.] 21st.*, 1983 (1988).
- 10 S. C. Wong and S. R. Turns, *Combust. Sci. Technol.* **66** (1-3), 75 (1989).
- 11 S. Y. Cho, F. Takahashi, and F. L. Dryer, *Combust. Sci. Technol.* **67** (1-3), 37 (1989).
- 12 F. Takahashi, I. J. Heilweil, and F. L. Dryer, *Combust. Sci. Technol.* **65** (1-3), 151 (1989).
- 13 S. J. Guisinger and M. E. Rippen, *Prepr. - Am. Chem. Soc., Div. Pet. Chem.* **34** (4), 885 (1989).
- 14 S. C. Wong and A. C. Lin, *Combust. Flame* **89** (1), 64 (1992).
- 15 H. S. Chung, C. S. H. Chen, R. A. Kremer, J. R. Boulton, and G. W. Burdette, *Energy Fuels* **13** (3), 641 (1999).
- 16 M. S. Fedorova, Y. V. Denisov, and V. K. Potapov, *Russ. J. Phys. Chem.* **47**, 1498 (1973).
- 17 A. A. Popov, N. N. Blinov, N. S. Vorob'eva, G. E. Zaikov, and S. G. Karpova, *Kinet. Katal.* **22** (1), 139 (1981).
- 18 R. C. Inman and M. P. Serve, *Org. Mass Spectrom.* **17** (5), 220 (1982).
- 19 R. Herzschuh, H. Kuehn, and M. Muehlstaedt, *J. Prakt. Chem.* **325** (2), 256 (1983).
- 20 M. V. Nesterov, V. A. Ivanov, V. M. Potekhin, and A. I. Grigor'ev, *Zh. Prikl. Khim. (Leningrad)* **57** (5), 1102 (1984).
- 21 Y. T. Lin, C. Lin, K. Liou, S. S. Cheng, and M. J. Chang, *J. Chin. Chem. Soc. (Taipei)* **33** (4), 341 (1986).
- 22 M. Brossi and C. Ganter, *Helv. Chim. Acta* **71** (4), 848 (1988).
- 23 W. V. Steele, R. D. Chirico, S. E. Knipmeyer, and N. K. Smith, Report No. Report, 1989.
- 24 F. A. Williams, R. K. Hanson, and C. Segal, *JANNAF 24th Airbreathing Propulsion Subcommittee and 36th Combustion Subcommittee Joint Meeting, 1999, Vol. 1* **692**, 151 (1999).
- 25 D. F. Davidson, D. C. Horning, J. T. Herbon, and R. K. Hanson, in *Proc. Combust. Inst.* (2000), Vol. 28, pp. 1687.
- 26 Z. Li, J. Eckwert, A. Lapicki, and S. L. Anderson, *Int. J. Mass Spectrom. Ion Processes* **167/168**, 269 (1997).
- 27 Z. Li and S. L. Anderson, *J. Phys. Chem. A* **102**, 9202 (1998).
- 28 S. E. Stein, director, in *NIST Chemistry WebBook, NIST Standard Reference Database Number 69*, edited by W. G. Mallard and P. J. Linstrom (NIST Mass Spec Data Center, National Institute of Standards and Technology, Gaithersburg MD 20899 (<http://webbook.nist.gov>), 2000).
- 29 M. J. Frisch, G. W. Trucks, H. B. Schlegel, G. E. Scuseria, M. A. Robb, J. R. Cheeseman, V. G. Zakrzewski, J. A. Montgomery, R. E. Stratmann, J. C. Burant, S. Dapprich, J. M. Millam, A. D. Daniels, K. N. Kudin, M. C. Strain, O. Farkas, J. Tomasi, V. Barone, M. Cossi, R. Cammi, B. Mennucci, C. Pomelli, C. Adamo, S. Clifford, J. Ochterski, G. A. Peterson, P. Y. Ayala, Q. Cui, K. Morokuma, D. K. Malick, A. D. Rabuck, K. Raghavachari, J. B. Foresman, J. Cioslowski, J. V. Ortiz, B. B. Stefanov, G. Liu, A. Liashenko, P. Piskorz, I. Komaromi, R. Gomperts, R. L. Martin, D. J. Fox, T. Keith, M. A. Al-Laham, C. Y. Peng, A. Nanayakkara, C. Gonzalez, M. Challacombe, P. M. W. Gill, B. G. Johnson, W. Chen, M. W. Wong, J. L. Andres, M. Head-Gordon, E. S. Replogle, and J. A. Pople, *GAUSSIAN 98*. (Gaussian, Inc., Pittsburgh PA, 1998).
- 30 S. G. Lias, J. F. Liebman, and R. D. Levin, *J. Phys. Chem. Ref. Data* **13**, 695 (1984).
- 31 M. S. Fedorova, Y. V. Denisov, and V. K. Potapov, *Zh. Fiz. Khim.* **47** (10), 2667 (1973).

- 32 Y. Ikezoe, S. Matsuoka, M. Takebe, and A. Viggiano, *Gas phase ion-molecule reaction rate*  
33 *constants through 1986*. (Mass Spec. Soc. of Japan (Distrib. by, Tokyo, 1987).
- 34 T. Su and M. T. Bowers, in *Gas Phase Ion Chemistry*, edited by M. T. Bowers (Acad. Pr., New  
35 York, 1979), Vol. 1, pp. 83.
- 36 T. A. Flaim and P. D. Ownby, *Journal of Vacuum Science and Technology* **8** (5), 661 (1971).
- 37 H. Nishimura and H. Tawara, *Journal of Physics B: Atomic, Molecular and Optical Physics* **27**  
38 (18), 4401 (1994).
- 39 San Diego Mechanism web page, Center for Energy Research (Combustion Division), University  
40 of California at San Diego (2004).
- 41 A. E. Lutz, R. J. Kee, and J. A. Miller, 1988.
- 42 R. J. Kee, F. M. Rupley, and J. A. Miller, 1989.
- 43 A. Violi, S. Yan, E. G. Eddings, A. F. Sarofim, S. Granata, T. Faravelli, and E. Ranzi,  
44 *Combustion Science & Technology* **174**, 399 (2002).
- 45 M. A. Banares, *Catalysis Today* **51** (2), 319 (1999).
- 46 R. J. Farrauto, *ACS Symposium Series* **766** (Green Engineering), 149 (2001).
- 47 P. Gelin and M. Primet, *Applied Catalysis, B: Environmental* **39** (1), 1 (2002).
- 48 G. Groppi, C. Cristiani, and P. Forzatti, *Catalysis* **13**, 85 (1997).
- 49 C. Lunot, *Journal de Physique IV: Proceedings* **12** (Pr2, Matériaux pour les Energies Propres), 25  
50 (2002).
- 51 J. G. McCarty, M. Gusman, D. M. Lowe, D. L. Hildenbrand, and K. N. Lau, *Catalysis Today* **47**  
52 (1-4), 5 (1999).
- 53 P. O. Thevenin, A. G. Ersson, H. M. J. Kusar, P. G. Menon, and S. G. Jaras, *Applied Catalysis,*  
54 *A: General* **212** (1-2), 189 (2001).
- 55 W. Lin, Y. X. Zhu, N. Z. Wu, Y. C. Xie, I. Murwani, and E. Kemnitz, *Applied Catalysis, B:*  
56 *Environmental* **50** (1), 59 (2004).
- 57 M. Lyubovsky, L. L. Smith, M. Castaldi, H. Karim, B. Nentwick, S. Etemad, R. LaPierre, and W.  
58 C. Pfefferle, *Catalysis Today* **83** (1-4), 71 (2003).
- 59 S. Pengpanich, V. Meeyoo, T. Rirksomboon, and K. Bunyakiat, *Applied Catalysis, A: General*  
**234** (1-2), 221 (2002).
- K. Persson, P. O. Thevenin, K. Jansson, J. Agrell, S. G. Jaras, and L. J. Pettersson, *Applied*  
*Catalysis, A: General* **249** (1), 165 (2003).
- C.-K. Shi, L.-F. Yang, and J.-X. Cai, *Chemistry Letters* **32** (1), 50 (2003).
- P. O. Thevenin, A. Alcalde, L. J. Pettersson, S. G. Jaras, and J. L. G. Fierro, *Journal of Catalysis*  
**215** (1), 78 (2003).
- K.-l. Yu, C.-j. Liu, Y.-p. Zhang, F. He, X.-l. Zhu, and B. Eliasson, *Plasma Chemistry and Plasma*  
*Processing* **24** (3), 393 (2004).
- I. Yuranov, P. Moeckli, E. Suvorova, P. Buffat, L. Kiwi-Minsker, and A. Renken, *Journal of*  
*Molecular Catalysis A: Chemical* **192** (1-2), 239 (2003).
- M. Alifanti, R. Auer, J. Kirchnerova, F. Thyron, P. Grange, and B. Delmon, *Applied Catalysis,*  
*B: Environmental* **41** (1-2), 71 (2003).
- W. B. Li, Y. Lin, and Y. Zhang, *ACS Symposium Series* **852** (Utilization of Greenhouse Gases),  
366 (2003).
- M. F. Wilkes, P. Hayden, and A. K. Bhattacharya, *Journal of Catalysis* **219** (2), 286 (2003).
- Z. Li, D. Peiris, J. Eckwert, and S. L. Anderson, in *Proceedings of the Ninth ONR Propulsion*  
*Meeting* (Naval Research Laboratory, Washington DC, 1996), pp. 145
- Z. Li and S. L. Anderson, *J. Phys. Chem. A* **107**, 1162 (2003).